Luminescence dating of buried cobble surfaces from sandy beach ridges

a case study from Denmark

Souza, Priscila E.; Sohbati, Reza; Murray, Andrew S.; Kroon, Aart; Clemmensen, Lars B.; Hede, Mikkel U.; Nielsen, Lars

Published in:
Boreas

DOI:
10.1111/bor.12402

Publication date:
2019

Document version
Publisher's PDF, also known as Version of record

BOREAS An international journal of Quaternary research

Luminescence dating of buried cobble surfaces from sandy beach ridges: a case study from Denmark

PRISCILA E. SOUZA, REZA SOHBATI, ANDREW S. MURRAY, AART KROON, LARS B. CLEMMENSEN, MIKKEL U. HEDE AND LARS NIELSEN

BOREAS

Souza, P. E., Sohbati, R., Murray, A. S., Kroon, A., Clemmensen, L. B., Hede, M. U. & Nielsen, L. 2019 (October): Luminescence dating of buried cobble surfaces from sandy beach ridges: a case study from Denmark. *Boreas*, Vol. 48, pp. 841–855. https://doi.org/10.1111/bor.12402. ISSN 0300-9483.

Here we investigate the use of optically stimulated luminescence (OSL) for dating cobbles from the body of successive beach ridges and compare cobble surface-derived ages to standard quartz OSL ages from sand. Between four and eight cobbles and sand samples (age control) were dated with the luminescence method, taken from the modern beach and from beach ridges on the south and north extremes of a prograding spit on the westernmost coast of Lolland, Denmark. Luminescence-depth profiles perpendicular to the surfaces of the cobbles show that the feldspar infrared signals stimulated at 50 °C were fully reset to various depths into the cobbles prior to final deposition; as a result, the equivalent doses determined from close to the surface of such cobbles can be used to calculate burial ages. Beach-ridge burial ages given by the average of ages of individual cobbles taken from the same site are consistent, within errors, with the ages derived from the sand samples. Cobble- and sand-derived ages show that the southernmost beach ridge at Albuen was formed around 2 ka ago, indicating that this sandy spit is younger than other coastal systems in Denmark. The agreement between ages derived from clasts and from standard quartz OSL in this study confirms that, even in the absence of sandy sediments, we can reliably date sites using OSL by targeting larger clasts. In addition, the record of prior light exposure contained in the shape of the cobbles' luminescence-depth profile removes one of the major uncertainties (i.e. the degree of signal reset prior to burial) in the luminescence dating of high latitude sites.

Priscila E. Souza (pes@ign.ku.dk), Aart Kroon, Lars B. Clemmensen, Mikkel U. Hede and Lars Nielsen, Department of Geosciences and Natural Resource Management, Faculty of Science, University of Copenhagen, Øster Voldgade 10, Copenhagen 1350, Denmark; *Present address: Tårnby Gymnasium og HF, Tejn Alle 5, Kastrup 2770, Denmark; Reza Sohbati, DTU Nutech, Technical University of Denmark, Roskilde DK-4000, Denmark; Andrew S. Murray, Nordic Laboratory for Luminescence Dating, Department of Geoscience, Aarhus University, RisøDTU campus, Copenhagen DK-4000, Roskilde, Denmark;* *received 10th January 2019, accepted 20th April 2019.*

Optically stimulated luminescence (OSL) ages are based on the measurement of trapped charge in the defects in mineral crystals such as quartz and feldspars. When these minerals are exposed to daylight, the trapped charge is released in the form of luminescence, with an intensity proportional to the time that has elapsed since the last exposure to daylight (Aitken 1998). OSL dating of sand-sized material is a well-established technique and has been successfully applied in many archaeological and geological studies (e.g. Fuchs & Owen 2008; Rittenour 2008; Wintle 2008; Thrasher *et al.* 2009; Clemmensen *et al.* 2012, 2018; Lampe & Lampe 2018). However, using sand-sized material may be challenging in some environments. For example, the latent luminescence signal in dating glacial and related sediments may, in some cases, not be completely reset by daylight during the last transport prior to deposition (e.g. Fuchs & Owen 2008; Rittenour 2008). The completeness of signal bleaching prior to burial of sand grains is difficult to assess directly, and partial bleaching remains a significant source of uncertainty in OSL dating of sand-sized grains (e.g. Olley *et al.* 1999). In addition, if the sedimentary unit of interest does not contain any sand- or silt-sized material, it cannot be dated using conventional luminescence dating techniques. As a result, it has been difficult to apply conventional OSL dating to, for instance, scree slopes, block fields and gravelly beach ridges.

Recently, several studies have demonstrated the potential of using large clasts in OSL dating (e.g. Simms *et al.* 2011, 2018; Sohbati *et al.* 2011, 2015; Simkins *et al.* 2013). These studies relied on the exposure of the clast surface to daylight, and the resulting resetting of the latent luminescence to some depth into the clast interior. Because the mineral grains in the cobble matrix are fixed (in contrast to sands, which is usually transported as individual grains), this resetting profile is preserved after burial, at least in part. Thus, larger clasts preserve a record of their bleaching prior to burial, and this information is contained in the shape of the luminescence-depth profile into the rock surface (e.g. Freiesleben *et al.* 2015; Sohbati *et al.* 2015; Jenkins *et al.* 2018). This is a major advantage compared to sediment dating using sand-sized grains, which do not record such information.

Here we test the application of luminescence rock surface dating to the surface of buried cobbles in sandy beach ridges to determine the time of deposition. We first assess the degree of bleaching, and then compare the cobble burial ages with those based on the OSL from sand-sized quartz extracted from the material surrounding the cobbles.

[Correction added on 21 June 2019, after first online publication: Corrections updated in tables 2-5]

DOI 10.1111/bor.12402

Study area and sampling sites

Albuen is located at the westernmost end of the island of Lolland, Denmark (Fig. 1A, B). It is a complex S–N orientated prograding spit (Fig. 1C) mainly formed by longshore currents in a microtidal environment (mean tidal range <10 cm; Danish Meteorological Institute 2018). The spit is ~5 km long with a hook-shaped recursive tip on the north and made up of a succession of beach ridges built from a mixture of cobbles and sand (Fig. 1C). Such beach ridges are relict berms, typical coastal features deposited mainly by wave-related processes (e.g. Tanner 1995; Otvos 2000; Clemmensen & Nielsen 2010; Tamura 2012; Bendixen *et al.* 2013; Hede *et al.* 2015), and have been extensively studied for reconstructing coastal environments as well as for estimating relative sea-level variations using luminescence dating (e.g. Murray-Wallace *et al.* 2002; Nielsen *et al.* 2006, 2017; Bjørnsen *et al.* 2008; Clemmensen *et al.* 2012; Bendixen *et al.* 2013; Lampe & Lampe 2018). Albuen is located in the vicinity of the hinge line where the vertical land movement in response to isostatic adjustment since the last glaciation changes from positive to negative (Lambeck *et al.* 1998; Hansen *et al.* 2012; Nielsen *et al.* 2014). Although the exact location of this hinge line may have changed over time, Albuen is considered to be an important study area to constrain sea-level variation as well as for geodynamic models of southwest Scandinavia.

The beach ridges at Albuen have a low relief (<2 m, Fig. 1C). Seven successive beach ridges were selected for sampling (all for sand sampling and two for both cobbles and sand sampling, Fig. 1C). From 0 to ~70 cm below the surface, they are composed of sand with some dispersed rounded cobbles (Fig. 2A, B). No systematic grain-size analysis was carried out on the bulk matrix material, but it is estimated that cobbles constitute between 10 and 30% of the total volume. Beach ridges' sediment composition and morphology (width and height) depend on both sediment availability and wave-energy level at the time of (berm) deposition (Bendixen *et al.* 2013). Sand and cobbles can both be deposited under swash and backwash processes on the seaward side of the berm during elevated water levels. Sand is likely to have been deposited under moderate wave conditions, whereas cobbles are likely to have been transported and deposited under more high-energy wave conditions. The present-day beach is mainly sand, with dispersed rounded cobbles (Fig. 2C). Each ridge is presumably subject to deposition by wave action during several events of elevated water, before it is abandoned as a result of spit growth.

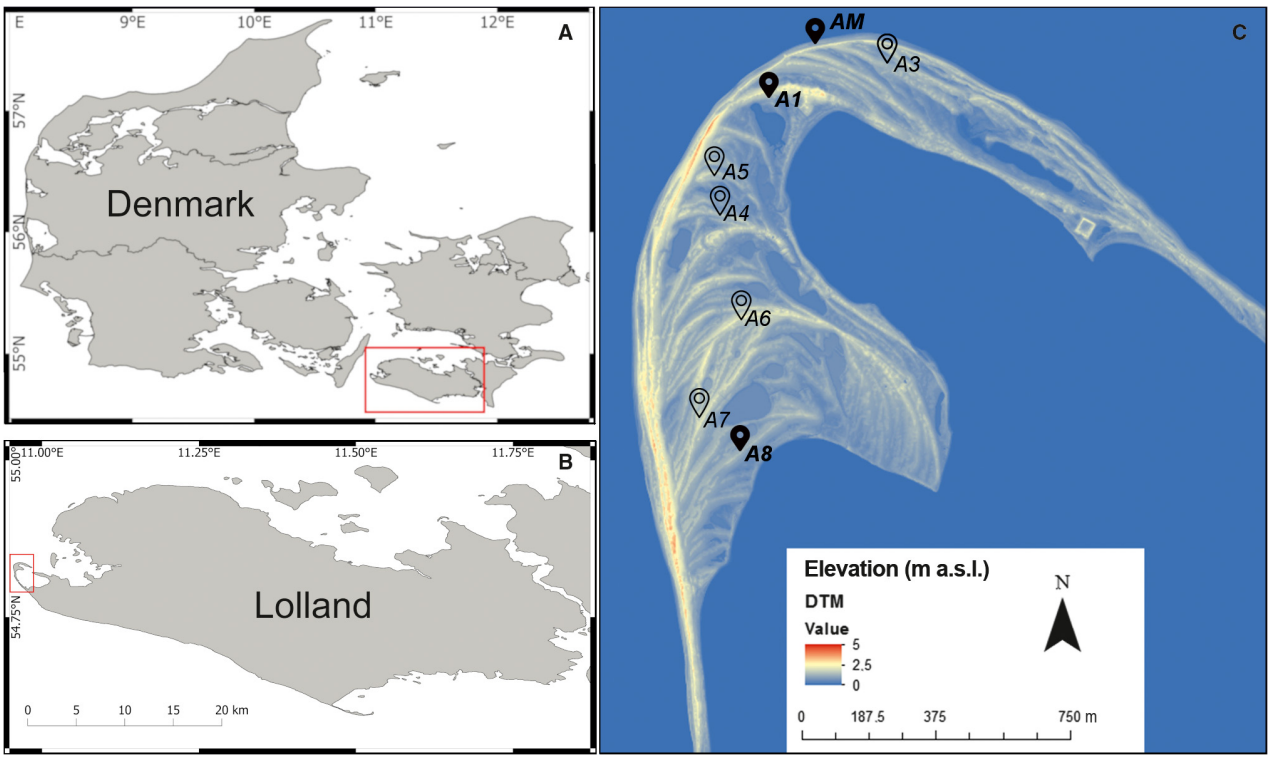

Fig. 1. Study area. A. Overview map of Denmark. The rectangle shows the sampling area on Lolland. B. Overview map of Lolland. The rectangle shows the sampling location on Albuen. C. Elevation map of Albuen showing the sampling sites. Sites that were dated using both cobbles and sand are labelled in bold font and with black filled location pins; hollow location pins indicate sites that were dated based on sand alone. [Colour figure can be viewed at www.boreas.dk]

Fig. 2. Pictures of sampling locations. A1 (A) and A8 (B) are ~70-cm-deep pits dug on the crest of the present-day beach-ridge surface. C. Modern beach (AM). View to the north. [Colour figure can be viewed at www.boreas.dk]

Material and methods

Sampling and sample preparation

Pits with dimensions of ~50×50×70 cm were dug into the crests of seven successive beach ridges (Fig. 1). From two beach ridges, A1 and A8 (black-filled pins in Fig. 1), both cobble and sand samples were collected. Cobbles were sampled by first digging a pit to a depth of about 60 cm, and then scraping into the base of the pit by hand, extracting a cobble surrounded by sand and placing it directly in a black plastic bag. This process took only a few seconds, and the cobble remained covered by sand during any possible light exposure. We do not believe there was any opportunity for significant surface bleaching during this process. At least 15 cobbles were randomly collected from 60 to 70 cm below the surface of the ridges A1 and A8. Sand samples were collected by hammering light-proof PVC tubes into the pit wall ~60 cm below the surface. Additionally, sand samples were collected, in the same manner as above, from other beach ridges between A1 and A8 (hollow pins in Fig. 1) to provide a chronological framework for the growth with time of the beach-ridge plain. Cobbles and sand were also taken from just below the surface (~10 cm) of the backshore of the modern beach (Fig. 2C) to investigate the degree of the resetting of the luminescence signal in samples that had been exposed to light immediately before the time of sampling (i.e. modern analogues). All the cobble surfaces are expected to have been frequently exposed to daylight as they were washed up and down on the beach by swash processes before final deposition at higher levels during high-energy events. Hereafter, we use the abbreviations 'AMsed' and 'AM*c*', where *c* is a number of identification for each cobble, to refer to sand and individual cobbles collected from the modern beach, respectively. Similarly, we use the abbreviations 'A*b*sed' and 'A*bc*', where *b* is the number of identification for each ridge (see Fig. 1C) and *c*

is again a number of identification for each cobble, to refer to sand and individual cobbles collected from the beach ridges, respectively. For example, the code for the sand sample from the beach ridge A8 is 'A8sed', and the code for a cobble from the same site will be 'A810' ('10' being the cobble identification number).

The environmental dose rate and the water content of sand samples were estimated using the material from the light-exposed ends of the PVC tubes used for sample collection. In the case of cobble samples, external dose rates were derived from measurements on the material that was collected with the cobbles, and it includes sand and other adjacent cobbles within the matrix.

Samples for luminescence measurements were prepared in the laboratory under low-level orange light (Sohbati *et al.* 2017). For sand samples, the fraction from the central part of the PVC tubes was used for equivalent dose (D_e) measurements. Quartz fractions were prepared following the standard procedure: wet sieving (180 to 250 μm), acid treatment (10% HCl for 60 min, 10% H_2O_2 for 60 min, 10% HF for 40 min and 10% HCl for 20 min). Quartz and feldspar grains were separated using heavy liquid (ρ = 2.62 g cm^{-3}), and the quartz grains were additionally etched using concentrated (~40%) HF for 40 min, followed by 10% HCl for 40 min. Only the quartz fraction of the sand material was used for luminescence measurements. No heavy mineral separation was performed because, in our experience, OSL signals from heavy minerals are invariably weak, and the mass fraction is very small.

Small chips were taken from the surface of each cobble for a preliminary sensitivity test, to select those with infrared signals >10^3 cts 0.2 s^{-1} (in response to a test dose of ~2 Gy. Cores of ~10 mm in diameter and up to ~25 mm long were then drilled from the selected cobbles using a diamond-tipped, water-cooled core drill. Cores were sliced into ~1.2-mm-thick slices at intervals of 1.5 mm using a low-speed water-cooled saw equipped with a diamond-tipped blade with a thickness of 0.3 mm. No chemical treatment was performed on the cobble slices. Variations in slice thickness are estimated to be <100 μm; laboratory beta dose rate uncertainties introduced by such variation are likely to be <±1.5% (based on Hansen *et al.* 2018: fig. 2).

After drilling, remaining cobble pieces and the material from around each cobble (~200 g per site) were prepared separately for high-resolution gamma spectrometry following the standard procedures: pulverizing, heating to 450 °C for 24 h to remove organic material (only for associated material) and casting with wax to provide a reproducible counting geometry and to prevent radon loss (Murray *et al.* 2018).

Instrumentation and measurement protocols

All luminescence measurements were carried out using a Risø TL/OSL reader (Model TL-DA 20) equipped with a calibrated ^{90}Sr/^{90}Y beta source. Large aliquots (~ 8 mm) of quartz extracted from sand samples were mounted on stainless-steel cups with silicone oil for OSL measurements. Luminescence signals were stimulated using blue diodes (λ = 470 nm, 80 mW cm^{-2}) and detected through a Hoya U-340 glass filter. Whole cobble slices were mounted directly on a reader carousel for discs for OSL measurements (Sohbati *et al.* 2011). K-feldspar signals were stimulated with IR diodes (λ = 875 nm, 135 mW cm^{-2}) and detected through a Schott BG39/BG3 filter combination (2 and 4 mm, respectively).

A single-aliquot regenerative (SAR) protocol (Murray & Wintle 2003) was used for quartz OSL measurements. Quartz extracts were heated to 200 °C for 10 s and to 180 °C for 0 s after giving the natural/regenerative and test doses, respectively, and stimulated with blue diodes at 125 °C for 40 s (Table 1). High-temperature blue-light stimulation at 280 °C was also performed at the end of each cycle for 40 s to remove any residual luminescence (Murray & Wintle 2003). OSL signal intensities were calculated using the initial 0.32 s of the signal minus an immediate background derived from the following 0.32 s. Cobble slices were measured using a post-IR IRSL SAR protocol (e.g. Buylaert *et al.* 2009). The slices were preheated to 200 °C for 100 s after giving both the natural/regenerative and test doses, stimulated using IR diodes first at 50 °C (IR_{50}) and then at 180 °C ($pIRIR_{180}$), each for 200 s (Table 1). After heating to the measurement temperature, there was a 30-s pause before stimulation to minimize problems with thermal lag (Sohbati *et al.* 2011). At the end of each cycle, residual luminescence was minimized using IR stimulation at 205 °C for 200 s. IRSL signal intensities were derived from the initial 10 s of stimulation less a background from the last 10 s of stimulation. The suitability of our SAR protocols for the samples used here was examined using the standard tests suggested by Wintle & Murray (2006): dose recovery, recycling ratio and recuperation.

Environmental dose rates were determined by measuring the concentration of radionuclides (i.e. ^{238}U, ^{232}Th, ^{226}Ra and ^{40}K) using high-resolution gamma spectrometry (Murray *et al.* 1987, 2018). K-rich areas on the cobble slices were identified using a Bruker M4 Tornado micro-XRF spectrometer. The micro-XRF images of such areas were then used for assessing the grain size of K-rich feldspar grains following Rades *et al.* (2018).

OSL ages from sediment quartz extracts

Dose rate

Radionuclide concentrations were converted to dose rate using conversion factors after Guérin *et al.* (2011). The matrix moisture content absorbs radiation and thus reduces the dose rate. We accounted for this effect by averaging the field water content and the laboratory estimate of saturation water content for each sample. The

Table 1. Outline of the SAR OSL and post-IR IRSL measurement protocols used for quartz grains and cobble slices, respectively. All measurements above 200 °C were carried out in nitrogen atmosphere.

Step	Quartz Treatment	Rock slices Treatment
1	Dose	Dose
2	Preheat 200 °C for 10 s	Preheat 200 °C for 100 s
3	Blue OSL (125 °C for 40 s) → L_x	IRSL (50 °C for 200 s) → L_x
3b	–	pIR IRSL (180 °C for 200 s) → L_x
4	Test dose	Test dose
5	Preheat 180 °C for 0 s	Preheat 200 °C for 100 s
6	Blue OSL (125 °C for 40 s) → T_x	IRSL (50 °C for 200 s) → T_x
6b	–	pIR IRSL (180 °C for 200 s) → T_x
7	Clean-out (blue OSL at 280 °C for 40 s	Clean-out (IRSL at 205 °C for 200 s)
8	Return to step 1	Return to step 1

cosmic ray dose rate was calculated following Prescott & Hutton (1994), and an internal alpha dose rate contribution of 0.010±0.002 Gy ka^{-1} in quartz from Vandenberghe *et al.* (2008). Radionuclide concentrations and calculated total dose rates are summarized in Table 2.

Luminescence characteristics and equivalent dose

The OSL signal from sediment quartz extracts (Fig. S1) is dominated by the fast component (e.g. Jain *et al.* 2003; Singarayer & Bailey 2003). The purity of the quartz was tested using the so-called IR OSL depletion ratio (Duller 2003), in which IR stimulation at room temperature is inserted before the blue OSL for a repeated regeneration dose. Pure quartz is effectively insensitive to IR stimulation at room temperature (e.g. Spooner 1994; Duller 2003) and so any loss of blue-stimulated signal detected in UV resulting from prior stimulation with IR is presumed to be associated with feldspar contamination. We checked the quartz purity of three aliquots per sample and the average ratio of the post-IR blue-stimulated signal to the blue-stimulated signal without prior IR stimulation was 0.97±0.01 (n = 20), indicating that any feldspar contamination of our blue-stimulated signal was negligible. To test the ability of our protocol to measure a known dose (dose recovery, Murray 1996), five aliquots per sample were optically bleached twice in the reader using blue diodes at room temperature for 40 s, with a pause of 10 000 s between bleaching to allow for any charge transferred to shallow traps to thermally decay; these bleached aliquots were then given a dose of ~3.5 Gy. The ratio of the average measured dose to the given dose was 1.01±0.02 (n = 31), indicating that our chosen protocol is able to accurately measure a known dose given in the laboratory before any thermal treatment.

Equivalent doses were measured for at least 30 aliquots per sample (except for the modern analogue for which 18 aliquots were measured); the arithmetic mean of the distribution was used in further calculations (Guérin *et al.* 2017). Aliquots with recycling ratio >10% from a unity and/or recuperation >5% of the natural signal were dismissed and not included in the D_e estimation. Figure S1 shows a typical quartz OSL dose response curve for our samples. Average D_e values of accepted aliquots ranged from 0.07±0.01 Gy (n = 16; modern beach sample) to 3.10±0.07 Gy (n = 48; beach ridge A8). As mentioned earlier, the degree of signal bleaching prior to final deposition cannot be directly assessed in sandy samples, but a modern analogue can be used to infer it. Assuming that the sand-sized sediment on the beach ridges at Albuen had experienced the same processes that the modern sand is subject to today, the relatively low D_e mean value measured from the modern sand sample suggests that beach-ridge sand was probably well bleached prior to final deposition. Average D_e values are given in Table 2.

Table 2. Summary of OSL ages from sediment quartz extracts.

Sample	D_e (Gy)	n	Dose rate (Gy ka^{-1})	Age (ka)
AMsed	0.07±0.01	16	1.68±0.07	0.04±0.01
A1sed	0.99±0.03	47	1.51±0.06	0.66±0.04
A3sed	0.37±0.01	31	1.60±0.07	0.23±0.01
A4sed	1.16±0.04	36	1.24±0.06	0.93±0.06
A5sed	1.37±0.04	37	1.65±0.07	0.83±0.05
A6sed	1.69±0.05	34	1.56±0.06	1.08±0.06
A7sed	1.89±0.05	41	1.18±0.04	1.60±0.09
A8sed	3.10±0.07	48	1.38±0.05	2.25±0.12

Ages

The OSL ages of quartz extracted from the beach ridges where cobbles were also collected (A8 and A1) are 2.25±0.12 ka (n = 48) and 0.66±0.04 ka (n = 47), respectively. Quartz OSL ages of the other assessed beach ridges are given in Table 2 and Fig. 3. Sand ages show that the beach-ridge system becomes younger towards the north (Fig. 3). The calculated age for the modern beach samples is 0.04±0.01 ka (n = 16) indicating that the effect of any residual signal in our samples is likely to be very small.

Luminescence characteristics of cobbles

In order to test the sensitivity of the quartz grains within our cobble samples, cobble slices were (i) stimulated with blue diodes at high temperature (220 °C for 100 s) in order to deplete the natural quartz and feldspar signals, (ii) given a dose (of ~11 Gy), (iii) stimulated with IR diodes at room temperature (at 50 °C for 100 s) to deplete the feldspar signal and then stimulated with the blue LEDs (at 125 °C for 40 s) and signals detected in UV. The observed OSL signals do not contain any fast component and decay very slowly, indicating that the quartz grains in our samples are not suitable for dating (Fig. 4A, B). The $pIRIR_{180}$ signals are generally anomalous, first rising to a maximum after

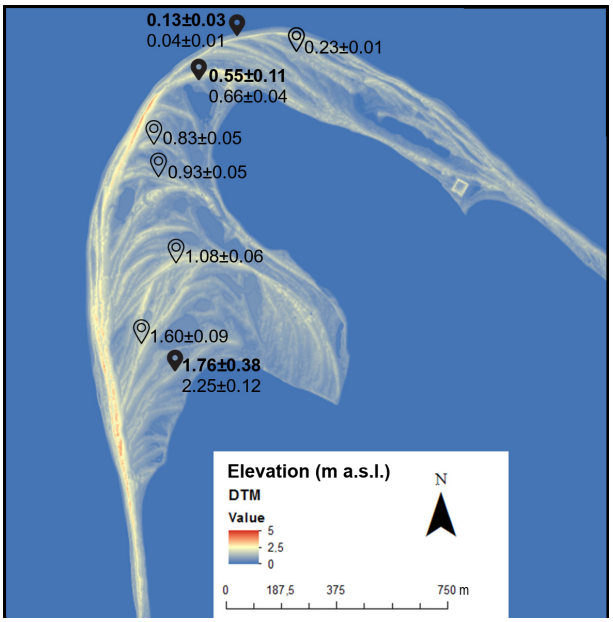

Fig. 3. Elevation map of Albuen showing final luminescence ages of each site. Black filled pins correspond to sites that were dated using both cobble surfaces (ages in bold) and sand. Hollow pins correspond to sites dated with sand alone. All ages are presented in thousands of years (ka) ago. [Colour figure can be viewed at www.boreas.dk]

about 25 s of stimulation before decreasing slowly (Fig. 4C, D). Such behaviour is likely to arise from an underlying isothermal thermoluminescence (ITL) signal (Fig. S2). Preliminary tests showed that a pause time of >1000 s before the stimulation was necessary to minimize this problem; this was considered impractical. Although for consistency we used a $pIRIR_{180}$ protocol, with an IR_{50} first stimulation, for all samples, we do not consider the $pIRIR_{180}$ signals further in our study. Slices from most of the cobbles examined here emitted strong IR_{50} signals (Fig. 4C, D), and 18 cobbles were selected in total for further investigations: four from the modern beach, six from A1 and eight from A8.

Luminescence-depth profiles

As discussed above, one of the advantages of luminescence rock surface dating compared to conventional sediment dating using sand is that solid granular matrices retain a record of the extent to which the latent luminescence signal was reset prior to final burial (e.g. Freiesleben *et al.* 2015; Sohbati *et al.* 2015; Jenkins *et al.* 2018). To investigate this, we measured the natural sensitivity-corrected signal (L_n/T_n) as a function of depth into the selected cobbles. Due to their small size, we were able to drill cores through the samples to investigate the variation of the luminescence signal from one surface of the cobble to the opposite surface. Figure 5 shows the luminescence-depth profiles from two different cobbles from each site. Note that the *y*-axis of the plots on the left side of Fig. 5 differs from that on the right side. In the examples shown on the left panels, L_n/T_n increases with depth and reaches a plateau (the so-called field saturation level) in the middle of the cobble. In the examples on the right panels this plateau is not reached, presumably because light exposure has been sufficiently long to at least partially bleach the latent IR_{50} signal throughout the cobble. For those samples that show field saturation in the middle of the cobble, the L_n/T_n values of all slices of the luminescence-depth profiles are normalized to the average L_n/T_n of the slices in field saturation. For those samples that did not reach field saturation, the L_n/T_n values of all slices were normalized to a laboratory-induced saturation level. In the cobbles from the modern beach AM, the IR_{50} signal at the surface of both sides of both cobbles is small; no significant difference is observed in the degree of resetting of these surfaces of individual cobbles (Fig. 5A, B). Also, the L_n/T_n does not increase significantly from the first (surface) to the second slice. These observations are consistent with the expectation that these cobbles had not been buried for a long time before sampling, and that all surfaces must have been well bleached as the cobbles had been repeatedly exposed to light by wave action in the swash zone before deposition. In the case of AM03, the IR_{50} signal increases with depth and reaches field saturation level in the middle of the cobble (Fig. 5A). In contrast, the luminescence-depth profile in cobble AM12 does not reach a plateau in the middle of the cobble, suggesting that the IR_{50} signal has been bleached, at least to some degree, throughout this cobble (Fig. 5B).

Profile shapes similar to those observed in the cobbles from the modern beach were observed from the cobbles collected from the beach ridges A1 (Fig. 5C, D) and A8 (Fig. 5E, F). The difference, however, is that the IR_{50} signal at the surface of these cobbles is not negligible but starts at some finite value (Fig. 5C–F; see also Chapot *et al.* 2012; Freiesleben *et al.* 2015; Sohbati *et al.* 2015). This surface signal results from the dose that these surfaces are presumed to have absorbed since deposition.

Dose recovery and D_e

In order to determine whether or not our chosen protocol is able to measure a known dose in these cobble samples, the natural luminescence signals of four inner slices from two cobbles from each site (i.e. from AM, A1, and A8) were optically bleached for 48 h (24 h each side) using a Hönle SOL2 solar simulator. Two slices from each cobble were then given a dose of ~21 Gy and measured in the usual manner; the other two slices were measured without any additional dose to give an estimate of any residual dose. The ratio of the average measured dose (less the respective average residual dose) to the given dose was then calculated to give the dose recovery ratio. The residual dose for IR_{50} signal, averaged over all cobbles, was 1.10±0.18 Gy (n = 15), and the dose recovery ratio

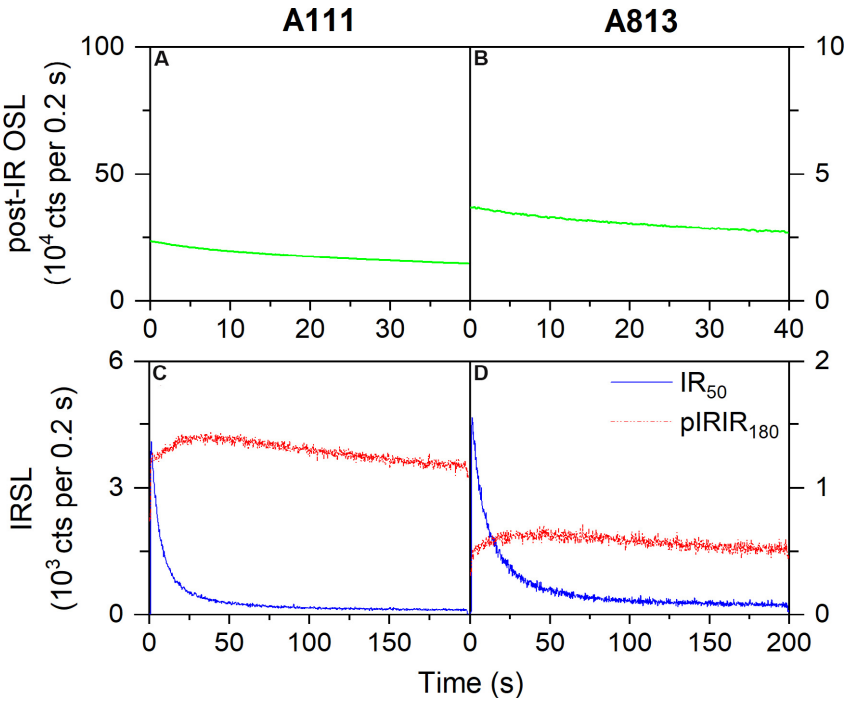

Fig. 4. Typical stimulation curves observed in the sensitivity test. A and B show the typical decay of the laboratory signal during a post-IR blue stimulation (i.e. for quartz sensitivity detection), and C and D during infrared stimulations at 50 °C (IR_{50}) and 180 °C ($pIRIR_{180}$) (for feldspar sensitivity detection). [Colour figure can be viewed at www.boreas.dk]

was 0.96±0.01 (n = 14). We conclude that we are able to measure with sufficient accuracy a known laboratory dose given to a previously unheated cobble slice using our SAR protocol.

Equivalent doses were measured from as many surface slices (depth ≤1.5 mm) as possible. For some of the cobbles, we could only get two or three surface slices (*n*) due to their small size: A113 (n = 2); A805, A813, A814 and A815 (n = 3). The surface D_e distributions from each site are shown in Fig. 6. Average D_e values from samples AM, A1 and A8 were 0.38±0.06 Gy (n = 21), 1.61±0.17 Gy (n = 24) and 4.11±0.23 Gy (n = 33), respectively. Relative standard deviation (RSD) values ranged from 30 to 70% (Fig. 6). Given that the calculated uncertainty of D_e from individual aliquots is of the order of a few percent, these samples are considerably overdispersed. It is implicit in our treatment that different surface slices from the same cobble are exposed to the same dose rate, and so this overdispersion is surprising. We are confident that it does not arise from incomplete bleaching (see above), but presumably at least some originates from variations in effective dose rate, including variations in effective grain size, K concentration, and possibly variability in the efficiency of luminescence sensitivity between different radiation types (Buylaert *et al.* 2018). It is for these reasons that we adopt the recommendations of Guérin *et al.* (2017) and derive the arithmetic average of the dose distributions for further calculations.

Cobble surface burial ages

Dose rate

Radionuclide concentrations measured with high-resolution gamma spectrometry were converted to infinite matrix dose rate data using the conversion factors of Guérin *et al.* (2011). The internal total beta dose rate to K-feldspar grains from ^{40}K and ^{87}Rb, calculated assuming an effective ^{40}K content of 12.5±0.5% (Huntley & Baril 1997), a ^{87}Rb content of 400±100 ppm (Huntley & Hancock 2001) and an average grain size of 400 μm, is 1.522±0.064 Gy ka^{-1}. An internal alpha dose rate in K-feldspars of 0.10±0.05 Gy ka^{-1} derived from the internal contribution of ^{238}U and ^{232}Th (Mejdahl 1987) was also included in the dose rates. The cosmic ray dose rate was calculated following Prescott & Hutton (1994) assuming a rock density of 2.65 g cm^{-3}, which is the mode density of all types of rocks (Johnson & Olhoeft 1984) and seems to be appropriate for the type of cobbles we are dating (Fig. 7).

The total effective environmental dose rate ($\dot{D}_{total}$) to the surface of the cobbles was estimated by summing the relevant contributions of the cosmic radiation and beta and gamma dose rates (Sohbati *et al.* 2015). Although the water content of the cobbles is negligible, the surrounding sandy material does contain water, and so the infinite-matrix dose rates need to be corrected for water content. This was based on that calculated using the sandy material taken from the ends of the sand sampling PVC tubes (see

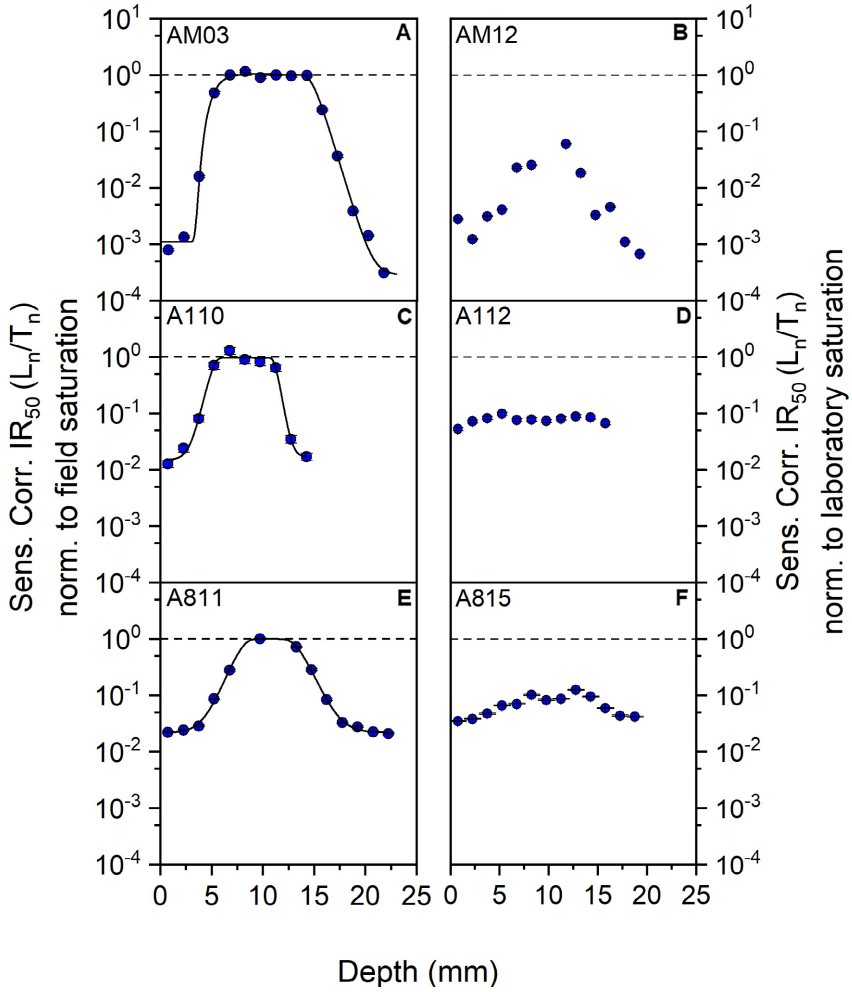

Fig. 5. Cobble luminescence-depth profiles normalized to saturation levels. Profiles A, C and E reach a plateau region in the middle of the cobble, indicating field saturation level (dashed horizontal line). Profiles B, D and F are from samples that, even in the middle, have been, at least partially, bleached by daylight; these are normalized to the laboratory saturation level (dashed horizontal line). Note that the extremes in the *x*-axes represent opposing surfaces of the cobbles. [Colour figure can be viewed at www.boreas.dk]

above). For each cobble, the total beta ($\dot{D}\beta_{total}$) and total gamma ($\dot{D}\gamma_{total}$) dose rates were derived by summing the contributions of the cobble itself ($\dot{D}\beta_{cobble}$ and $\dot{D}\gamma_{cobble}$) and from its associated material ($\dot{D}\beta_{sand}$ and $\dot{D}\gamma_{sand}$). These percentage contributions were estimated as follows. Since the matrices in which the cobbles were embedded were mainly sandy (cobbles were not touching each other, Fig. 2), we estimated the variation of the total beta dose rate at the cobble/sediment interface based on Aitken (1985: appendix H) using the attenuation factor from Sohbati *et al.* (2015), as:

$$\dot{D}\beta_{total} = 0.5\dot{D}\beta_{cobble} + 0.5\dot{D}\beta_{cobble}\left(1 - e^{-bx}\right) + 0.5\dot{D}\beta_{sand}e^{-bx} \quad (1)$$

$\dot{D}\beta_{cobble}$ (Gy ka^{-1}) is the cobble (dry) infinite-matrix beta dose rate, $\dot{D}\beta_{sand}$ (Gy ka^{-1}) is the water-content-corrected infinite-matrix beta dose rate from the material associated with each cobble, $\times$ (mm) is the depth into cobble from the cobble/sand interface, and b (1.9 mm^{-1}) is the beta linear attenuation coefficient in the cobble (Sohbati *et al.* 2015). The first term in Equation 1 represents half of the $\dot{D}\beta_{cobble}$ present at the surface of the cobble (because the cobble is much thicker than the range of beta particles), and the second term represents the build-up of the remainder of the $\dot{D}\beta_{cobble}$ with depth into the cobble. The third term represents the attenuation with distance into the cobble of 50% of the $\dot{D}\beta_{sand}$ present at the surface of the cobble. Equation 1 was integrated over the depth of the surface slice (1.2 mm) and divided by this thickness to give the average beta dose rate. It is thus estimated that $\sim$80% of the cobble (dry) infinite-matrix β dose rate ($\dot{D}\beta_{cobble}$) contributes to the total beta dose rate to the first slice ($\dot{D}\beta_{total}$); this is supplemented by $\sim$20% of the surrounding material infinite-matrix β dose rate ($\dot{D}\beta_{sand}$). For cobbles <12 cm in diameter, the contribution of $\dot{D}\gamma_{cobble}$ to $\dot{D}\gamma_{total}$ is given with sufficient accuracy by the product of the cobble density (g cm^{-3}) and diameter

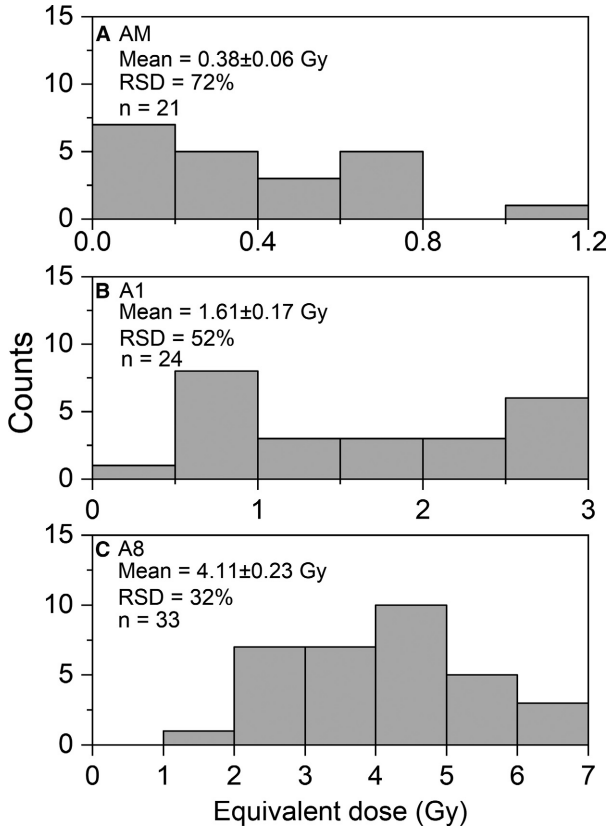

Fig. 6. Equivalent dose distributions derived from surface slices of (A) the modern beach, (B) beach ridge A1, and (C) beach ridge A8 cobbles. Errors on the mean correspond to standard error; RSD = relative standard deviation (or coefficient of variation); n = number of accepted aliquots (each aliquot corresponds to a cobble surface slice).

(cm) (Aitken 1985); the resulting value is taken as the percent contribution. Assuming an average cobble density of 2.65 g cm^{-3} and an average cobble diameter of 5.3 cm (given an average cobble dimension of 10×4×2 cm), ~14% of the (dry) $\dot{D}\gamma_{cobble}$ and ~86% of the water-content-corrected infinite-matrix gamma dose rate of the associated material ($\dot{D}\gamma_{sand}$) contribute to $\dot{D}\gamma_{total}$. Table 3 summarizes the data on the environmental dose rate calculations.

Uncorrected ages

The IR_{50} cobble surface burial ages were simply derived by dividing the cobble surface D_e values (without subtracting any residuals; see above) by the effective dose rate at the surface of the cobbles (see above). It is, however, known that the IR_{50} signal from feldspars is unstable; a phenomenon that is known as 'anomalous fading' (Wintle 1973). As a result, the ages prior to fading corrections are regarded as minimum ages (Table 4).

Fading correction

Anomalous fading was quantified using two different approaches: the conventional g value measurements (Huntley & Lamothe 2001) and the saturation ratio (Rades *et al.* 2018).

The g value expresses the fading rate as a percentage of IR signal loss with storage time after irradiation (Huntley & Lamothe 2001; Fig. S3). Three inner slices from each cobble were reset in the reader using an IR stimulation at 205 °C for 200 s, and then L_x/T_x cycles were repeatedly measured, both immediately after irradiation, and after a delay time of 12 h (inserted after the preheat; Auclair *et al.* 2003). Average g values for all samples were >6% dec.$^{-1}$ (Fig. 8), giving age corrections in excess of 50%. Measured g values from A1 samples varied the most, ranging from 1.8±1.4 to 13.9±1.6% dec.$^{-1}$.

The saturation ratio is an alternative approach to fading correction that has been recently proposed by Rades *et al.* (2018); this is specifically suitable for rock samples because they often contain a record of field saturation level in the innermost (unbleached) part of their luminescence profile, identified by a plateau. Field saturation is where the accumulation of latent luminescence as a result of dose rate is matched by the fading rate, so that the luminescence signal ceases to change with time. In this method, a fading correction factor can be derived by dividing the L_n/T_n value from slices from the field saturated plateau part of the profile by the corresponding laboratory saturation level (L_{sat}/T_{sat}) measured using the same slices after giving them a high saturating dose (i.e. >>1 kGy) in the laboratory (Rades *et al.* 2018). Because Albuen cobbles are small, many are at least partially reset even at the cobble centre. Only seven out of 18 cobbles were identified as in field saturation in the middle and were deemed suitable for this fading correction approach. We first measured the natural IR_{50} signal of a saturated inner slice to determine L_n/T_n. The measured slice was then given a dose of ~4200 Gy using a ^{60}Co gamma source and re-measured to give L_{sat}/T_{sat}. The field-to-laboratory saturation ratio was then derived by dividing the L_n/T_n by its respective L_{sat}/T_{sat}. Table 4 shows calculated field-to-laboratory saturation ratios. Three samples out of seven give ratios above 1. Since such ratios are not physically meaningful, this suggests that the measurement uncertainty is significantly larger than that based on calculations, and we note that the mean of the five largest ratios is 1.09±0.10, indistinguishable from unity. As a result, we only consider ratios of <0.5 to be significantly different from unity, and the only two samples meeting this criterion are A111 and A805.

Corrected ages

The ages for all the samples were corrected using both cobble-specific (g_{cobble}) and average g values ($g_{average}$). In addition, the ages of two samples (A111 and A805) were corrected using field-to-laboratory saturation ratios (see

Table 3. Environmental dose rate information for the cobble and sand samples. Cobbles' $\dot{D}_{total}$ includes the contribution of effective beta and gamma dose rates from both cobble and associated sand. Dose rates in feldspar assume a K concentration of 12.5±0.5% for 400 μm K-feldspar grains (Huntley & Baril 1997).

Sample	^{226}Ra (Bq ka^{-1})	^{232}Th (Bq ka^{-1})	^{40}K (Bq ka^{-1})	Water content (%)	Beta dose rate (Gy ka^{-1})	Gamma dose rate (Gy ka^{-1})	$\dot{D}_{total}$ (Gy ka^{-1})
AM02	39.4±1.4	67.6±1.6	2059.4±41.9	0	6.05±0.11	2.69±0.05	6.78±0.11
AM03	6.1±0.5	8.8±0.6	112.7±7.2	0	0.41±0.02	0.24±0.01	2.76±0.08
AM04	39.6±1.9	196.7±2.2	1407.7±35.0	0	5.29±0.09	3.71±0.05	6.42±0.10
AM12	7.7±0.6	8.0±0.6	441.8±14.4	0	1.25±0.04	0.50±0.02	3.34±0.09
AMsed	10.1±0.5	9.4±0.5	426.9±11.1	14±4	0.93±0.03	0.74±0.02	1.68±0.07
A109	47.6±1.9	86.3±2.0	1341.3±31.5	0	4.45±0.09	2.41±0.05	5.56±0.10
A110	17.1±2.9	51.0±3.2	1444.3±51.1	0	4.16±0.13	1.86±0.06	5.30±0.12
A111	24.3±1.2	47.5±1.3	1320.1±32.1	0	3.90±0.08	1.77±0.04	5.11±0.10
A112	20.9±1.3	54.0±1.4	1802.5±30.9	0	5.12±0.08	2.20±0.04	5.97±0.10
A113	28.5±1.4	48.7±1.4	1244.3±31.1	0	3.76±0.08	1.75±0.04	5.02±0.10
A116	43.7±2.4	40.0±2.1	830.8±41.7	0	2.80±0.11	1.43±0.06	4.36±0.11
A1sed	9.82±0.4	9.9±0.4	382.3±10.9	13±4	0.87±0.02	0.63±0.01	1.51±0.06
A805	11.5±1.5	34.6±1.5	1342.9±43.7	0	3.74±0.11	1.55±0.04	4.92±0.11
A807	55.7±2.0	72.7±1.9	1038.2±38.0	0	3.67±0.10	2.06±0.06	4.95±0.10
A809	36.6±2.4	47.3±2.1	1423.5±46.1	0	4.28±0.12	1.94±0.06	5.33±0.11
A811	14.3±0.8	21.6±0.8	452.4±16.9	0	1.43±0.04	0.71±0.02	3.30±0.09
A812	16.1±1.1	23.3±1.2	53.6±12.1	0	0.45±0.03	0.43±0.02	2.63±0.08
A813	14.5±1.0	16.5±1.1	938.6±28.8	0	2.63±0.07	1.04±0.03	4.13±0.09
A814	43.8±1.0	69.1±1.1	468.2±16.4	0	2.09±0.05	1.49±0.04	3.84±0.09
A815	45.3±1.7	41.8±1.6	3878.4±60.3	0	10.52±0.16	3.86±0.06	9.66±0.13
A8sed	7.0±0.3	8.6±0.3	370.1±10.3	15±4	0.80±0.02	0.58±0.01	1.38±0.05

above). All uncorrected and corrected ages are given in Table 4. In general, average corrected ages from each site have a relative standard deviation of >40%, regardless of the fading correction approach (Table 4). Ages corrected using g_{cobble} are not statistically different from the ages corrected with $g_{average}$; only $g_{average}$ corrected ages will be discussed further. The final average ages from AM, A1 and A8 are 0.13±0.03, 0.55±0.11 and 1.76±0.38 ka, respectively. Final ages of samples A111 and A805 given by the field-to-laboratory saturation ratios are 0.69±0.04 and 1.29±0.10 ka, respectively; these are consistent with the respective $g_{average}$ corrected ages (Table 4).

The importance of the assumed grain size

In the calculation of dose rates, we assumed an average K-feldspar grain size of 400 μm to allow us to calculate both the attenuation of the external beta dose rate, and the

Table 4. Cobble IRSL D_e values and uncorrected and corrected ages using the cobble-specific (g_{cobble}) and site-averaged ($g_{average}$) g values, and the field-to-laboratory saturation ratios. Cobble ages are corrected using the field-to-laboratory saturation ratio only in cases where the ratio is <0.5.

Sample	D_e (Gy)	n	Uncorrected age (ka)	g_{cobble} (% dec^{-1})	g_{cobble} corrected age (ka)	$g_{average}$ (% dec^{-1})	$g_{average}$ corrected age (ka)	Field to lab. sat. ratio	Sat. ratio corrected age (ka)
AM02	0.35±0.07	6	0.06±0.01	7.9±1.5	0.09±0.02	5.49±1.01	0.076±0.018	–	–
AM03	0.17±0.04	7	0.06±0.02	3.1±1.4	0.08±0.02	”	0.09±0.02	1.18±0.04	–
AM04	0.75±0.09	4	0.13±0.02	6.1±1.4	0.18±0.03	”	0.17±0.02	–	–
AM12	0.40±0.14	4	0.12±0.04	4.9±1.4	0.17±0.06	”	0.18±0.06	–	–
A109	0.74±0.13	6	0.15±0.03	10.9±1.8	0.33±0.15	7.19±2.16	0.23±0.08	–	–
A110	2.70±0.12	5	0.56±0.03	1.8±1.4	0.58±0.07	”	0.9±0.3	1.10±0.03	–
A111	1.63±0.05	3	0.35±0.01	10.8±2.0	0.8±0.5	”	0.58±0.19	0.46±0.02	0.69±0.04
A112	2.45±0.17	4	0.45±0.03	2.9±1.3	0.51±0.07	”	0.7±0.2	–	–
A113	1.03±0.09	2	0.22±0.02	13.9±1.6	0.8±0.3	”	0.36±0.12	–	–
A116	0.96±0.01	4	0.24±0.01	2.6±1.3	0.28±0.03	”	0.41±0.13	–	–
A805	2.32±0.16	5	0.51±0.04	11.1±1.6	1.4±0.7	6.37±1.13	0.80±0.13	0.36±0.01	1.29±0.10
A807	3.8±0.5	4	0.83±0.11	4.8±1.4	1.1±0.2	”	1.3±0.2	–	–
A809	3.3±0.3	4	0.67±0.06	9.4±1.6	1.5±0.5	”	1.05±0.19	–	–
A811	4.72±0.15	4	1.46±0.06	2.5±1.4	1.7±0.2	”	2.5±0.4	0.89±0.03	–
A812	5.4±0.2	4	2.03±0.12	2.6±1.8	2.6±0.5	”	3.7±0.7	0.86±0.03	–
A813	5.5±0.5	6	1.42±0.13	8.1±1.5	2.9±0.9	”	2.4±0.4	–	–
A814	3.16±0.13	3	0.86±0.04	4.5±1.3	1.19±0.19	”	1.4±0.2	1.4±0.1	–
A815	4.1±0.4	3	0.50±0.05	7.8±1.5	0.8±0.2	”	0.72±0.13	–	–

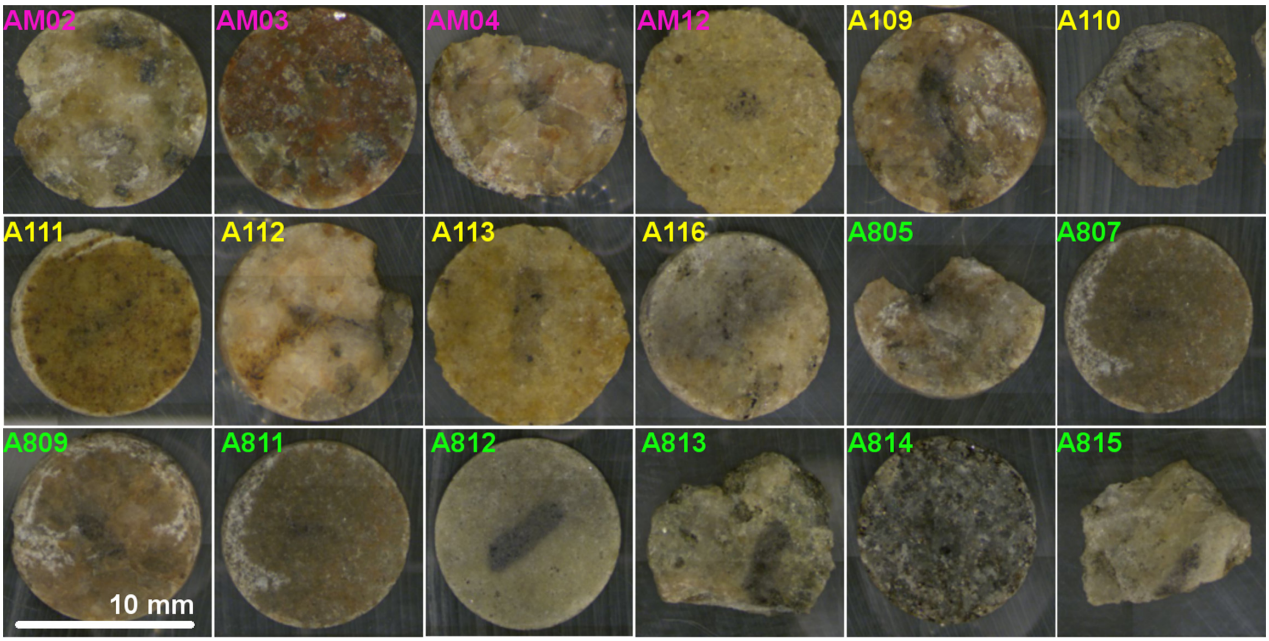

Fig. 7. Optical images of a surface slice from each cobble. [Colour figure can be viewed at www.boreas.dk]

build-up of the internal beta dose rate from ^{40}K and ^{87}Rb (see above). However, we have very little information about this grain size, and it is important to consider the effect of this assumption. For instance, had the assumed grain size been smaller, the beta dose rate contributions from internal ^{40}K and ^{87}Rb would also be smaller; this would tend to decrease the total dose rate ($\dot{D}_{total}$) and increase the final cobble age.

In order to investigate the effect of the grain-size assumption, we first attempted to estimate the actual average grain size of K-feldspar grains in our cobble slices and then assessed the sensitivity of the cobble ages to changes in the grain-size assumption. Micro-XRF images of surface and second slices of each sample show that K-rich areas vary considerably in size from sample to sample (see examples in Fig. S4). We selected the micro-XRF images of two extreme samples with apparent small (sample A811) and large (sample A815) constituent ^{40}K rich grains, in order to estimate the range of grain-size variation in our samples. Following Rades *et al.* (2018), we analysed these images to derive the grain-size distribution using Image J (Fig. S4). The resulting average ^{40}K rich grain diameters are 370±10 and 740±40 μm for samples A811 and A815, respectively. This implies that while for some samples the assumed grain size of 400 μm is valid, for others it can be underestimated by up to ~50% and so might have biased our cobble age estimations.

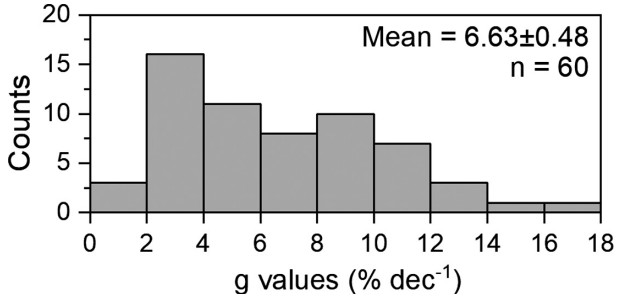

Fig. 8. Distribution of g values (% dec.$^{-1}$) from all cobbles.

We recalculated the ages of three cobbles from each site, assuming a range of grain diameters: 100, 200, 400, 1000 and 2000 μm. These cobbles were chosen to contain different measured bulk K concentrations (as measured by high-resolution gamma spectroscopy), and so different dose rates. As can be seen in Fig. 9, the higher the cobble dose rate, the less sensitive is the dose rate to the grain size (Fig. 9A), and thus the less dependent the cobble age is on the grain-size assumption (Fig. 9B). For example, the variation of $\dot{D}_{total}$ with grain size for sample A815 with high bulk K content (^{40}K = 3878 Bq kg^{-1}; Table 3) is small (Fig. 9A), while the $\dot{D}_{total}$ for sample A812 with low K content (^{40}K = 54 Bq ka^{-1}; Table 3) increases by a factor of ~3 from the grain size of 100 μm to the grain size 2000 μm (Fig. 9A). As a result, the ages show a similar trend in dependence on grain size where the samples with low radioactivity are the most sensitive (Fig. 9B; Table 5). The age of cobble A812, for example, ranges from 6.3±1.2 to 1.4±0.2 ka, for grain sizes of 100 and 2000 μm, respectively (Fig. 9B), whereas the ages of cobble A815 are indistinguishable for 100 and 2000 μm grains (0.72±0.13 and 0.83±0.16 ka, respectively, Fig. 9B).

Discussion

The luminescence-depth profiles of all sensitive cobbles are evidence that the latent IR_{50} luminescence signal was

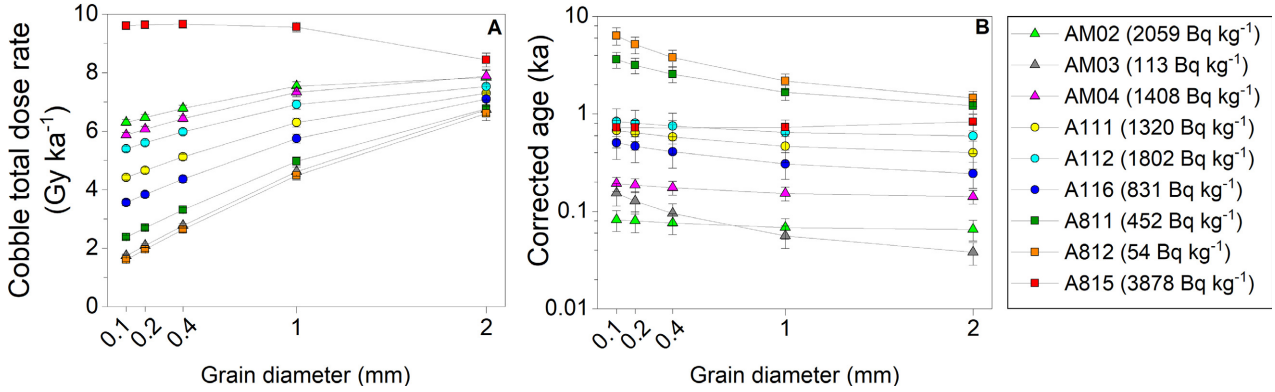

Fig. 9. Grain-size effect on dose rate and final ages. A. Cobble total beta dose rate ($\dot{D}_{total}$) as a function of grain diameter for three representative samples from each site. B. The fading-corrected ages of the cobbles as a function of grain size. The values in the legend refer to the K concentration of the cobble as measured by high-resolution gamma spectrometry. [Colour figure can be viewed at www.boreas.dk]

fully bleached, at least at the cobble surfaces. In some cobbles the IR_{50} signal has been bleached to some degree throughout the cobble. Other studies have reported similar observation of bleaching to depths >20 mm (e.g. Sohbati *et al.* 2012; Ou *et al.* 2018; Gliganic *et al.* 2019), although these were usually observed in visibly translucent samples, such as quartzite.

On average, cobble ages are within errors, in agreement with respective quartz OSL ages from the sandy material surrounding the rocks (age control; Fig. 10) despite (i) the significant scatter in D_e estimates of aliquots from the same cobble surface, (ii) age estimates based on an assumed grain size (400 μm), and (iii) high fading correction factors. Simkins *et al.* (2015) have also reported significant overdispersion in aliquot D_e of cobble quartz grains, and they also obtained ages that agreed with independent age control (Simkins *et al.* 2013). Here, IR_{50} signals from cobbles taken from the modern beach gave ages about a hundred years older than those based on quartz OSL from the surrounding sand (Fig. 10).

Analysis of the size of ^{40}K rich areas using micro-XRF data suggests that the grain size assumed in the dose rate calculations was not necessarily appropriate for all samples. Nevertheless, we have shown that the importance of the grain-size assumption on the final ages is dependent on the ^{40}K concentration of the cobble (Fig. 9). At least from the dosimetry perspective, it may be preferable to work with high K concentration cobbles because they show less dependence on the assumed grain size. Nevertheless, the sample that was almost pure K-feldspar (according to its measured bulk K concentration, sample A815) provided an age about ~35% of the expected value (based on A8sed, see Tables 2 and 4). Our results probably reflect the observations of Buylaert *et al.* (2018); they investigated the dose recorded by single- and multi-grain aliquots of feldspars, and showed that the relationship between K concentration, grain volume and apparent dose rate is more complex than previously understood.

Despite these difficulties, the average IR_{50} cobble ages are generally consistent, within errors, with the quartz OSL ages of the surrounding sand. Both cobble and sand ages show that the oldest beach ridges on Albuen were formed in the south and that the beach-ridge system has developed towards the north over a time period of ~2000 years (Fig. 3, Tables 2, 4). The number of major beach ridges formed between A8 and A1 during an average time period of ~1400 years is about 10; this indicates that each major beach ridge records sedimentation of about 140 years, between the initial building of the berm and its final abandonment. The presence of minor beach ridges between the major ones indicates that the 'true' time period of formation for the major ridges is <140 years, and may be as short as a few decades. Even so this would support our earlier expectation that the major beach ridges in Albuen are the result of several episodes of elevated water level deposition. Also, the error bars on the luminescence ages of both sand and cobble samples are larger than the formation time of the investigated ridges, at least in the case of the older ones. Thus, even if cobbles and

Table 5. Ratios of final ages assuming a grain size of 2000 μm to final ages assuming a grain size of 100 μm.

Sample	^{40}K (Bq kg^{-1})	$\frac{\text{Final age}_{\varphi=2000\,\mu m}}{\text{Final age}_{\varphi=100\,\mu m}}$
A812	53.62	0.23
AM03	112.70	0.25
AM12	441.81	0.34
A811	452.44	0.33
A814	468.21	0.41
A116	830.79	0.48
A813	938.55	0.46
A807	1038.16	0.57
A113	1244.25	0.58
A111	1320.07	0.59
A109	1341.29	0.65
A805	1342.93	0.57
AM04	1407.67	0.74
A809	1423.47	0.63
A110	1444.31	0.62
A112	1802.48	0.71
AM02	2059.43	0.80
A815	3878.37	1.14

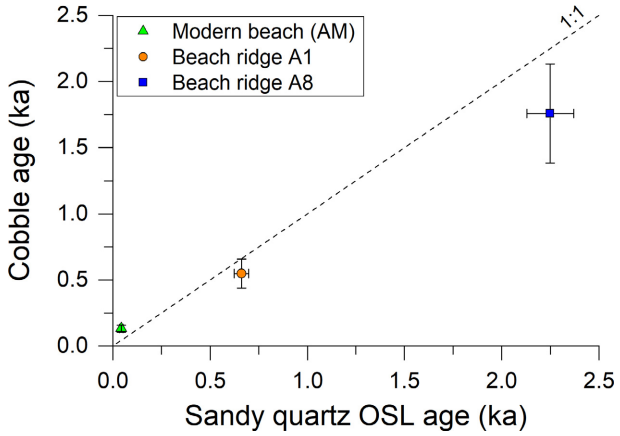

Fig. 10. Quartz OSL vs. cobble IRSL ages. Cobble ages correspond to the average of the $g_{average}$ corrected cobble ages of each site. [Colour figure can be viewed at www.boreas.dk]

sand were deposited during different events and buried within weeks of each other, their ages should be indistinguishable.

The beach-ridge system in Albuen is noticeably younger than other beach-ridge systems in the region, most of which initiated 4500–7000 years ago (Clemmensen *et al.* 2012, 2018; Hede *et al.* 2015). However, Lampe & Lampe (2018) have studied another beach-ridge plain in NE Germany, also close to the hinge line of isostatic adjustment, which began to form around 2000 years ago; this is when the Holocene relative sea-level rise in the region slowed down significantly, although with some minor fluctuations. The causes of the progradation of Albuen over the last 2000 years are not yet fully understood, but are probably due to changes in the intensity of the longshore transport of sediments from the south, and to sediment availability and accommodation space in the pre-existing glacial topography of the seabed.

Conclusions

In this study we have investigated the use of cobble surfaces as chronometers by examining the luminescence ages of buried cobbles taken from beach ridges and the modern beach on the westernmost coast of Lolland, Denmark. Clast-specific burial doses and dosimetry were used to derive apparent ages for those cobbles identified as well bleached, based on their luminescence profiles with depth. We conclude that, although the effective environmental dose rates are complex and not yet fully understood, the average ages of individual cobbles provide depositional ages consistent with those based on more conventional dating of the surrounding sandy material. This demonstrates that similar sites can be dated reliably using the luminescence from cobble surfaces. This is particularly important because it opens up the possibility of determining the depositional history of more challenging areas that lack materials for conventional OSL dating.

Acknowledgements. – We acknowledge funding by the Brazilian Government's program Science without Borders (CNPq), the Independent Research Fund Denmark and Geocenter Denmark. We thank Sigurd Bohr and Peer Torben Jørgensen for their assistance during the fieldwork. Further, we thank Dr. Regina DeWitt and an anonymous reviewer for their comments on an earlier version of this manuscript, which greatly helped improve the manuscript.

Author contributions. – PES, LN, AK and ASM designed the research in discussion with RS, LBC and MUH. PES, ASM and MUH collected the sediment samples for luminescence dating. PES processed the samples, performed all luminescence measurements, and analysed and discussed the data with RS and ASM. Protocols for measuring cobbles were designed by PES, RS and ASM. PES wrote the article with contributions from all co-authors.

Data availability statement. – Boreas encourages authors to share the data and other artefacts supporting the results in the paper by archiving it in an appropriate public repository. Authors may provide a data availability statement, including a link to the repository they have used, in order that this statement can be published in their paper. Shared data should be cited.

References

Aitken, M. J. 1985: *Thermoluminescence dating*. 359 pp. Academic Press, London.

Auclair, M., Lamoth, M. & Huot, S. 2003: Measurement of anomalous fading for feldspar IRSL using SAR. *Radiation Measurements 37*, 487–492.

Bendixen, M., Clemmensen, L. & Kroon, A. 2013: Sandy berm and beach-ridge formation in relation to extreme sea-levels: a Danish example in a micro-tidal environment. *Marine Geology 344*, 53–64.

Bjørnsen, M., Clemmensen, L. B., Murray, A. & Pedersen, K. 2008: New evidence of the Littorina transgressions in the Kattegat: optically stimulated luminescence dating of a beach ridge system on Anholt, Denmark. *Boreas 37*, 157–168.

Buylaert, J.-P., Murray, A. S., Thomsen, K. J. & Jain, M. 2009: Testing the potential of an elevated temperature IRSL signal from K-feldspar. *Radiation Measurements 44*, 560–565.

Buylaert, J.-P., Újvári, G., Murray, A., Smedley, R. & Kook, M. 2018: On the relationship between K concentration, grain size and dose in feldspar. *Radiation Measurements 120*, 181–187.

Chapot, M. S., Sohbati, R., Murray, A. S., Pederson, J. L. & Rittenour, T. M. 2012: Constraining the age of rock art by dating a rockfall event using sediment and rock-surface luminescence dating techniques. *Quaternary Geochronology 13*, 18–25.

Clemmensen, L. B. & Nielsen, L. 2010: Internal architecture of a raised beach ridge system (Anholt, Denmark) resolved by ground-penetrating radar investigations. *Sedimentary Geology 223*, 281–290.

Clemmensen, L. B., Hougaard, I. W., Murray, A. S. & Pedersen, S. S. 2018: A high-resolution sea-level proxy dated using quartz OSL from the Holocene Skagen Odde spit system, Denmark. *Boreas 47*, 1184–1198.

Clemmensen, L. B., Murray, A. S. & Nielsen, L. 2012: Quantitative constraints on the sea-level fall that terminated the Littorina Sea Stage, southern Scandinavia. *Quaternary Science Reviews 40*, 54–63.

Danish Meteorological Institute. 2018: DMI. Available at: http://ocean.dmi.dk/tides/tides_dk.uk.php (accessed 23.08.2018).

Duller, G. A. T. 2003: Distinguishing quartz and feldspar in single grain luminescence measurements. *Radiation Measurements 37*, 161–165.

Freiesleben, T., Sohbati, R., Murray, A., Jain, M., al Khasawneh, S., Hvidt, S. & Jakobsen, B. 2015: Mathematical model quantifies multiple daylight exposure and burial events for rock surfaces using luminescence dating. *Radiation Measurements 81*, 16–22.

Fuchs, M. & Owen, L. A. 2008: Luminescence dating of glacial and associated sediments: review, recommendations and future directions. *Boreas 37*, 636–659.

Gliganic, L. A., Meyer, M. C., Sohbati, R., Jain, M. & Barrett, S. 2019: OSL surface exposure dating of a lithic quarry in Tibet: laboratory validation and application. *Quaternary Geochronology 49*, 199–204.

Guérin, G., Christophe, C., Philippe, A., Murray, A. S., Thomsen, K. J., Tribolo, C., Urbanova, P., Jain, M., Guibert, P., Mercier, N., Kreutzer, S. & Lahaye, C. 2017: Absorbed dose, equivalent dose, measured dose rates, and implications for OSL age estimates: introducing the Average Dose Model. *Quaternary Geochronology 41*, 163–173.

Guérin, G., Mercier, N. & Adamiec, G. 2011: Dose-rate conversion factors: update. *Ancient TL 29*, 5–8.

Hansen, J. M., Aagaard, T. & Binderup, M. 2012: Absolute sea levels and isostatic changes of the eastern North Sea to central Baltic region during the last 900 years. *Boreas 41*, 180–208.

Hansen, V., Murray, A., Thomsen, K., Jain, M., Autzen, M. & Buylaert, J.-P. 2018: Towards the origins of over-dispersion in beta source calibration. *Radiation Measurements 120*, 157–162.

Hede, M. U., Sander, L., Clemmensen, L. B., Kroon, A., Pejrup, M. & Nielsen, L. 2015: Changes in Holocene relative sea-level and coastal morphology: a study of a raised beach ridge system on Samsø, southwest Scandinavia. *The Holocene 25*, 1402–1414.

Huntley, D. J. & Baril, M. R. 1997: The K content of the K-feldspars being measured in optical dating or in thermoluminescence dating. *Ancient TL 15*, 43–46.

Huntley, D. J. & Hancock, R. G. 2001: The Rb contents of the K-feldspar grains being measured in optical dating. *Ancient TL 19*, 43–46.

Huntley, D. J. & Lamothe, M. 2001: Ubiquity of anomalous fading in K-feldspars and the measurement and correction for it in optical dating. *Canadian Journal of Sciences 38*, 1093–1106.

Jain, M., Murray, A. S. & Bøtter-Jensen, L. 2003: Characterisation of blue-light stimulated luminescence components in different quartz samples: implications for dose measurement. *Radiation Measurements 37*, 441–449.

Jenkins, G. T., Duller, G. A. T., Roberts, H. M., Chiverrell, R. C. & Glasser, N. F. 2018: A new approach for luminescence dating glaciofluvial deposits - High precision optical dating of cobbles. *Quaternary Science Reviews 192*, 263–273.

Johnson, G. R. & Olhoeft, G. R. 1984: Density of rocks and minerals. *In* Carmichael, R. S. (ed.): *Handbook of Physical Properties of Rocks*, 1–39. CRC Press, Boca Raton.

Lambeck, K., Smither, C. & Ekman, M. 1998: Tests of glacial rebound models for Fennoscandinavia based on instrumented sea- and lake-level records. *Geophysical Journal International 135*, 375–387.

Lampe, M. & Lampe, R. 2018: Evolution of a large Baltic beach ridge plain (Neudarss, NE Germany): a continuous record of sea-level and wind-field variation since the Homeric Minimum. *Earth Surface Processes and Landforms 43*, 3042–3056.

Mejdahl, V. 1987: Internal radioactivity in quartz and feldspar grains. *Ancient TL 5*, 10–17.

Murray, A. S. 1996: Developments in optically stimulated luminescence and photo-transferred thermoluminescence dating of young sediments: application to a 2000-year sequence of flood deposits. *Geochimica et Cosmochimica Acta 60*, 565–576.

Murray, A. S. & Wintle, A. G. 2003: The single aliquot regenerative dose protocol: potential for improvements in reliability. *Radiation Measurements 37*, 377–381.

Murray, A. S., Helsted, L. M., Jain, M. & Buylaert, J.-P. 2018: Measurement of natural radioactivity: calibration and performance of a high-resolution gamma spectrometry facility. *Radiation Measurements 120*, 215–220.

Murray, A., Marten, R., Johnston, A. & Martin, P. 1987: Analysis for naturally occurring radionuclides at environmental concentrations by gamma spectrometry. *Journal of Radioanalytical and Nuclear Chemistry 115*, 263–288.

Murray-Wallace, C. V., Banerjee, D., Bourman, R. P., Olley, J. M. & Brooke, B. P. 2002: Optically stimulated luminescence dating of Holocene relict foredunes, Guichen Bay, South Australia. *Quaternary Science Reviews 21*, 1077–1086.

Nielsen, L., Bendixen, M., Kroon, A., Hede, M. U., Clemmensen, L. C., Weβling, R. & Elberling, B. 2017: Sea-level proxies in Holocene raised beach ridge deposits (Greenland) revealed by ground-penetrating radar. *Scientific Reports 7*, 46460, https://doi.org/10.1038/srep46460.

Nielsen, A., Murray, A. S., Pejrup, M. & Elberling, B. 2006: Optically stimulated luminescence dating of a Holocene beach ridge plain in Northern Jutland, Denmark. *Quaternary Geochronology 1*, 305–312.

Nielsen, L., Hansen, J. M., Hede, M. U., Pejrup, M. & Noe-Nygaard, N. 2014: Simultaneous estimation of lithospheric uplift rates and absolute sea level change in southwest Scandinavia from inversion of sea level data. *Geophysical Journal International 199*, 1018–1029.

Olley, J. M., Caitcheon, G. G. & Roberts, R. G. 1999: The origin of dose distributions in fluvial sediments, and the prospect of dating single grains from fluvial deposits using optically stimulated luminescence. *Radiation Measurements 30*, 207–217.

Otvos, E. G. 2000: Beach ridges - definition and significance. *Geomorphology 32*, 83–108.

Ou, X. J., Roberts, H. M., Duller, G. A., Gunnb, M. D. & Perkinsa, W. T. 2018: Attenuation of light in different rock types and implications for rock surface luminescence dating. *Radiation Measurements 120*, 305–311.

Prescott, J. R. & Hutton, J. T. 1994: Cosmic ray contributions to dose rates for luminescence and ESR dating: large depths and long-term variations. *Radiation Measurements 23*, 497–500.

Rades, E. F., Sohbati, R., Lüthgens, C., Jain, M. & Murray, A. S. 2018: First luminescence-depth profiles from boulders from moraine deposits: insights into glaciation chronology and transport dynamics in Malta valley, Austria. *Radiation Measurements 120*, 281–289.

Rittenour, T. M. 2008: Luminescence dating of fluvial deposits: applications to geomorphic, palaeoseismic and archaeological research. *Boreas 37*, 613–635.

Simkins, L. M., DeWitt, R., Simms, A. R. & Shapiro, R. S. 2016: Investigation of optically stimulated luminescence behaviour of quartz from crystalline rock surfaces: a look forward. *Quaternary Geochronology 36*, 161–173.

Simkins, L. M., Simms, A. R. & DeWitt, R. 2013: Relative sea-level history of Marguerite Bay, Antarctic Peninsula derived from optically stimulated luminescence-dated beach cobbles. *Quaternary Science Reviews 77*, 141–155.

Simkins, L. M., Simms, A. & DeWitt, R. 2015: Assessing the link between coastal morphology, wave energy and sea ice throughout the Holocene from Antarctic raised beaches. *Journal of Quaternary Science 30*, 335–348.

Simms, A. R., DeWitt, R., Kouremenos, P. & Drewry, A. M. 2011: A new approach to reconstructing sea levels in Antarctica using optically stimulated luminescence of cobble surfaces. *Quaternary Geochronology 6*, 50–60.

Simms, A. R., Whitehouse, P. L., Simkins, L. M., Nield, G., DeWitt, R. & Bentley, M. J. 2018: Late Holocene relative sea levels near Palmer Station, northern Antarctic Peninsula, strongly controlled by late Holocene ice-mass changes. *Quaternary Science Reviews 199*, 49–59.

Singarayer, J. S. & Bailey, R. M. 2003: Further investigations of the quartz optically stimulated luminescence components using linear modulation. *Radiation Measurements 37*, 451–458.

Sohbati, R., Murray, A. S., Buylaert, J.-P., Almeida, N. A. & Cunha, P. P. 2012: Optically stimulated luminescence (OSL) dating of quartzite cobbles from the Tapada do Montinho archaeological site (east-central Portugal). *Boreas 41*, 452–462.

Sohbati, R., Murray, A. S., Jain, M., Buylaert, J.-P. & Thomsen, K. 2011: Investigating the resetting of OSL signal in rock surfaces. *Geochronometria 38*, 249–258.

Sohbati, R., Murray, A. S., Lindvold, L., Buylaert, J.-P. & Jain, M. 2017: Optimization of laboratory illumination in optical dating. *Quaternary Geochronology 39*, 105–111.

Sohbati, R., Murray, A. S., Porat, N., Jain, M. & Avner, U. 2015: Age of a prehistoric "Rodedian" cult site constrained by sediment and rock surface luminescence dating techniques. *Quaternary Geochronology 30*, 90–99.

Spooner, N. A. 1994: On the optical dating signal from quartz. *Radiation Measurements 23*, 593–600.

Tamura, T. 2012: Beach ridges and prograded beach deposits as palaeoenvironment records. *Earth-Science Reviews 114*, 279–297.

Tanner, W. F. 1995: Origin of beach ridges and swales. *Marine Geology 129*, 149–161.

Thrasher, I. M., Mauz, B., Chiverrell, R. C. & Lang, A. 2009: Luminescence dating of glaciofluvial deposits: a review. *Earth-Science Reviews 97*, 133–146.

Vandenberghe, D., Corte, F. D., Buylaert, J.-P., Kučerac, J. & Van den Hautea, P. 2008: On the internal radioactivity in quartz. *Radiation Measurements 43*, 771–775.
Wintle, A. G. 1973: Anomalous fading of thermo-luminescence in mineral samples. *Nature 245*, 143–144.
Wintle, A. G. 2008: Fifty years of luminescence dating. *Archaeometry 50*, 276–312.
Wintle, A. G. & Murray, A. S. 2006: A review of quartz optically stimulated luminescence characteristics and their relevance in single-aliquot regeneration dating protocols. *Radiation Measurements 41*, 369–391.

Supporting Information

Additional Supporting Information may be found in the online version of this article at http://www.boreas.dk.

Fig. S1. Typical quartz OSL dose response and stimulation (inset) curves from sample A8.

Fig. S2. Typical isothermal TL (black) and IRSL (grey) signals at 180 °C.

Fig. S3. Typical example of fading rate measurement for IR_{50} signal.

Fig. S4. Grain-size analysis based on the micro-XRF images of the first two slices from cobbles A811 (left column) and A815 (right column).